

MHD natural convection in an inclined cavity filled with a fluid saturated porous medium with heat source in the solid phase

M.A. Mansour¹, A.J. Chamkha², R.A. Mohamed³,
M.M. Abd El-Aziz³, S.E. Ahmed³

¹Department of Mathematics, Assuit University, Assuit, Egypt

²Manufacturing Engineering Department

The Public Authority for Applied Education and Training
Shuweikh 70654, Kuwait
achamkha@yahoo.com

³Department of Mathematics, South Valley University, Qena, Egypt

Received: 2009-03-22 **Revised:** 2009-09-29 **Published online:** 2010-03-04

Abstract. A numerical investigation of unsteady magnetohydrodynamic free convection in an inclined square cavity filled with a fluid-saturated porous medium and with internal heat generation has been performed. A uniform magnetic field inclined with the same angle of the inclination of the cavity is applied. The governing equations are formulated and solved by a direct explicit finite-difference method subject to appropriate initial and boundary conditions. Two cases were considered, the first case when all the cavity walls are cooled and the second case when the cavity vertical walls are kept adiabatic. A parametric study illustrating the influence of the Hartmann number, Rayleigh number, the inclination angle of the cavity and the dimensionless time parameter on the flow and heat transfer characteristics such as the streamlines, isotherms and the average Nusselt number is performed. The velocity components at mid section of the cavity as well as the temperature profiles are reported graphically. The values of average Nusselt number for various parametric conditions are presented in tabular form.

Keywords: natural convection, inclined cavity, porous medium, MHD, heat generation.

1 Introduction

The study of flow of an electrically-conducting fluid has many applications in engineering problems such as magnetohydrodynamics (MHD) generators, plasma studies, nuclear reactors, geothermal energy extraction and the boundary layer control in the field of aerodynamics [1, 2]. Specifically, Bejan and Khair [1] reported on the natural convection boundary layer flow in a saturated porous medium with combined heat and mass transfer. Lai and Kulacki [2] extended the problem of Bejan and Khair [1] to include wall fluid injection effects. Chamkha and Khaled [3] considered magnetic field and wall mass

transfer effects on coupled heat and mass transfer by natural convection from a vertical semi-infinite plate maintained at a constant heat flux.

Heat and fluid flows in a cavity that experiences convective heating or cooling at the surface are found in a wide variety of applications including lakes and geothermal reservoirs, underground water flow, solar collector, etc. [4]. Associated industrial applications include secondary and tertiary oil recovery, growth of crystals [5], heating and drying process [6–8], solidification of casting, sterilization, etc. Natural or free convection in a porous medium has been studied extensively. Cheng [9] provides a comprehensive review of the literature on free convection in fluid saturated porous media with a focus on geothermal systems. Oosthuizen and Patrick [10] performed numerical studies of natural convection in an inclined square enclosure with part of one wall heated to a uniform temperature and with the opposite wall uniformly cooled to a lower temperature and with the remaining wall portions. The enclosure is partially filled with a fluid and partly filled with a porous medium, which is saturated with the same fluid. The main results considered were the mean heat transfer rate across the enclosure. Nithiarasu et al. [11] examined the effects of variable porosity on convective flow patterns in side a porous cavity. The flow is triggered by sustaining a temperature gradient between isothermal lateral walls. It was found that the variation in porosity significantly affects natural flow convective pattern. Khanafer and Chamkha [12] performed numerical study of mixed convection flow in a lid driven cavity filled with a fluid-saturated porous media. In this study, the influence of the Richardson number, Darcy number and the Rayleigh number played an important role on mixed convection flow inside a square cavity filled with a fluid-saturated porous media. Nithiarasu et al. [13] examined effects of applied heat transfer coefficient on the cold wall of the cavity up on flow and heat transfer inside a porous medium. The differences between the Darcy and non-Darcy flow regime were clearly investigated for different Darcy, Rayleigh and Biot numbers and aspect ratio. Grosan et al. [14] discussed the effects of magnetic field and internal heat generation on the free convection in a rectangular cavity filled with a porous medium. The problem of effects of non-uniform porosity on double diffusive natural convection in a porous cavity with partially permeable wall was analyzed by Akbala and Bayta [15].

The main objective of this paper is to study the effects of an inclined magnetic field on the unsteady natural convection in an inclined cavity filled with a fluid saturated porous medium with heat source in the solid phase. The magnetic field is inclined on the cavity bottom with the same inclination angle of the cavity on the horizontal plane. The finite-difference method is employed to solve this problem. The present results are validated by favorable comparisons with previously published results. The streamline and isotherm shapes in the cavity for different values of the problem parameters are plotted and discussed. In addition, the velocity components in X and Y directions as well as the temperature profiles are illustrated and discussed.

2 Mathematical formulation

Consider unsteady laminar natural convection flow in inclined cavities with an electrically-conducting fluid-saturated porous medium with internal heat generation. In this problem,

the following assumptions have been made:

1. The cavity walls are kept to a constant temperature T_0 or the cavity vertical walls are adiabatic.
2. Properties of the fluid and the porous medium are isotropic and homogeneous everywhere.
3. The enclosure is permeated by a uniform inclined magnetic field.
4. The angle of inclination of the magnetic field B on the cavity bottom is the same angle of inclination of the cavity on the horizontal plane.
5. A uniform source of heat generation in the flow region with constant volumetric rate is considered.
6. The viscous, radiation and Joule heating effects are neglected.
7. The density is assumed to be a linear function of temperature ($\rho = \rho_0(1 - \beta(T - T_0))$).

The geometric and the Cartesian coordinate system are schematically shown in Fig. 1.

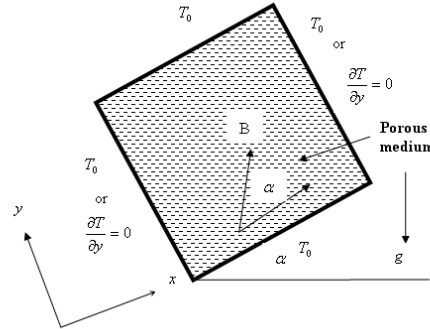


Fig. 1. Physical model of the problem.

Under the above assumptions, the governing equations are (see [15]):

$$\frac{\partial u}{\partial x} + \frac{\partial v}{\partial y} = 0, \quad (1)$$

$$\frac{\partial u}{\partial y} - \frac{\partial v}{\partial x} = \frac{g\beta k}{\nu} \left[\frac{\partial T}{\partial y} \sin \alpha - \frac{\partial T}{\partial x} \cos \alpha \right] + \frac{\sigma_0 k \beta_0^2}{\mu} \left[-\frac{\partial u}{\partial y} \sin^2 \alpha + 2\frac{\partial v}{\partial y} \sin \alpha \cos \alpha + \frac{\partial v}{\partial x} \cos^2 \alpha \right], \quad (2)$$

$$\sigma \frac{\partial T}{\partial t} + u \frac{\partial T}{\partial x} + v \frac{\partial T}{\partial y} = \alpha_m \left(\frac{\partial^2 T}{\partial x^2} + \frac{\partial^2 T}{\partial y^2} \right) + \frac{(1 - \varepsilon) q_0^m}{\rho c_p}. \quad (3)$$

The continuity equation is considered by defining a stream function $\psi(x, y)$, so that equation (2) can be written as

$$\frac{\partial^2 \psi}{\partial x^2} + \frac{\partial^2 \psi}{\partial y^2} = \frac{g\beta k}{\nu} \left[\frac{\partial T}{\partial y} \sin \alpha - \frac{\partial T}{\partial x} \cos \alpha \right] - \frac{\sigma_0 k \beta_0^2}{\mu} \left[\frac{\partial^2 \psi}{\partial y^2} \sin^2 \alpha + 2 \frac{\partial^2 \psi}{\partial x \partial y} \sin \alpha \cos \alpha + \frac{\partial^2 \psi}{\partial x^2} \cos^2 \alpha \right], \quad (4)$$

where $u = \partial\psi/\partial y$ and $v = -\partial\psi/\partial x$ and β_0 is the magnitude of B .

In this study, the following dimensionless variables are used for equations (3) and (4):

$$\begin{aligned} \Psi &= \frac{\psi}{\alpha_m}, \quad X = \frac{x}{l}, \quad Y = \frac{y}{l}, \quad U = \frac{l}{\alpha_m} u, \quad V = \frac{l}{\alpha_m} v, \\ \theta &= \frac{T - T_0}{\Delta T}, \quad \Delta T = \frac{q_0^m}{k} l^2, \quad \tau = \frac{\alpha_m}{l^2} t. \end{aligned} \quad (5)$$

Using these variables, the stream function and energy equations in non-dimensional form can be written as:

$$\frac{\partial^2 \Psi}{\partial X^2} + \frac{\partial^2 \Psi}{\partial Y^2} = Ra \left[\frac{\partial \theta}{\partial Y} \sin \alpha - \frac{\partial \theta}{\partial X} \cos \alpha \right] - Ha^2 \left[\frac{\partial^2 \Psi}{\partial Y^2} \sin^2 \alpha + 2 \frac{\partial^2 \Psi}{\partial X \partial Y} \sin \alpha \cos \alpha + \frac{\partial^2 \Psi}{\partial X^2} \cos^2 \alpha \right], \quad (6)$$

$$\left[\sigma \frac{\partial \theta}{\partial \tau} + \frac{\partial \Psi}{\partial Y} \frac{\partial \theta}{\partial X} - \frac{\partial \Psi}{\partial X} \frac{\partial \theta}{\partial Y} \right] = \frac{\partial^2 \theta}{\partial X^2} + \frac{\partial^2 \theta}{\partial Y^2} + (1 - \varepsilon), \quad (7)$$

where $Ra = (kg\beta l \Delta T)/(\nu\alpha)$ is the Rayleigh number, $Ha = \sigma_0 k \beta_0^2 / \mu$ is the Hartmann number for the porous medium and $\sigma = (\varepsilon(\rho c_p)_f + (1 - \varepsilon)(\rho c_p)_s)/(\rho c_p)_f$ is the heat capacity ratio.

The initial and boundary conditions for equations (6) and (7) are as follows:

$$\begin{aligned} \tau = 0: \quad & \Psi = 0, \quad \theta = 0 \quad \text{everywhere,} \\ \tau > 0: \quad & \Psi = 0, \quad \theta = 0 \quad \text{or} \quad \frac{\partial \theta}{\partial Y} = 0 \quad \text{at} \quad X = 0 \quad \text{and} \quad X = 1, \quad 0 \leq Y \leq 1, \\ \tau > 0: \quad & \Psi = 0, \quad \theta = 0 \quad \text{at} \quad Y = 0 \quad \text{and} \quad Y = 1, \quad 0 \leq X \leq 1. \end{aligned} \quad (8)$$

It should be noted that, in the second case with non-inclined cavity corresponds to Grosan et al. [14] case.

Once we know the temperature, we can obtain the rate of heat transfer at the right wall, which are given in terms of the average Nusselt number Nu which is defined as:

$$\overline{Nu} = - \int_0^1 \left(\frac{\partial \theta}{\partial X} \right) dy. \quad (9)$$

3 Solution technique

The numerical algorithm used to solve the dimensionless governing equations (6) and (7) with the boundary conditions (8) is based on the finite difference methodology. Central difference quotients were used to approximate the second derivatives in both the X - and Y -directions. The obtained discretized equations are then solved using a suitable algorithm. The numerical computations were carried out for (61×61) grid nodal points with a time step of 10^{-5} . The iteration process was terminated under the following condition:

$$\max |\lambda_{i,j}^{n+1} - \lambda_{i,j}^n| \leq 10^{-5}, \quad (10)$$

where λ is the general dependent variable which can stand for U , V , Ψ and θ . This method was found to be suitable and gave results that are very close to the numerical results obtained Grosan et al. [14]. From Figs. 2, we can observe an excellent agreement between our results and the results obtained by Grosan et al. [14]. This favorable comparison lends confidence in the numerical results to be reported subsequently.

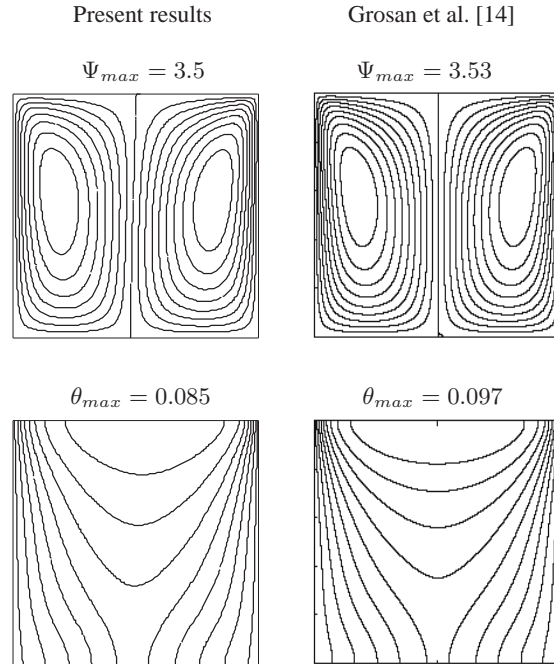


Fig. 2. Comparison between our results and Grosan et al. [14].

4 Results and discussion

In this section, numerical results for the contours of the streamlines and isotherms as well as selected velocity and temperature profiles at mid section of the cavity for various values of the cavity and magnetic field inclination angle α are presented. In addition, representative results for the average Nusselt number Nu for various conditions are presented in tabulated form and discussed. In all of these results, ε was fixed at a value of 0.6.

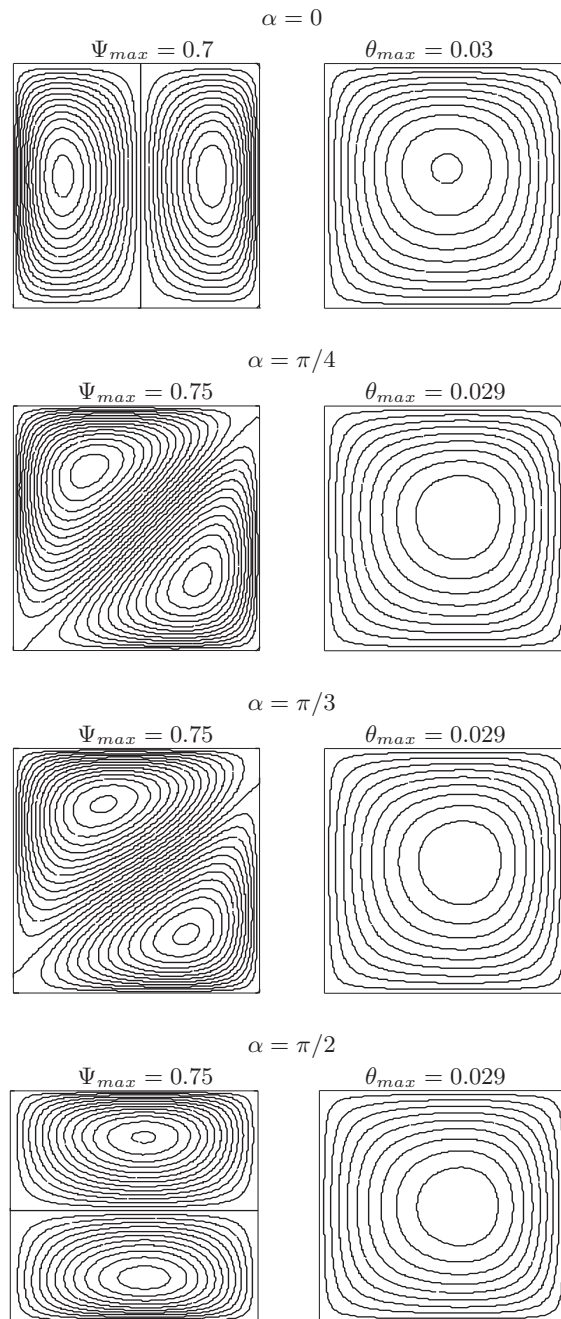
Case 1: The cavity walls are kept to a constant temperature T_0

Fig. 3 presents steady-state contours for the streamlines and isotherms for various values of the cavity and magnetic field inclination angle α ($0.0, \pi/4, \pi/3, \pi/2$) for a Rayleigh number $Ra = 500$ and a Hartmann number $Ha = 0.5$ when all the cavity walls are cooled. In general, for $\alpha = 0$ (non-inclined cavity), two vertically stretched separated recirculating cells or vortices in the whole enclosure exist. As the cavity inclination angle increases, these two cells tend to stretch along the inclination line for $\alpha = \pi/4$ and $\alpha = \pi/3$ until they become stretched horizontally when $\alpha = \pi/2$. In addition, the streamlines become crowded not only at the left wall but also at the right wall of the cavity which means that the velocity of the fluid increases in the immediate vicinity of these walls. It is observed that tilting the cavity by $\pi/4$ increases the flow movement and the maximum value of stream function increases to become $\Psi_{max} = 0.75$. However, further tilting of the cavity yields a reduction in the fluid velocity. It is also observed from Fig. 3 that the isotherms form a single anti-clockwise rotating cell through the whole cavity. This is an interesting behavior because this means that the walls of the cavity are hotter than any other region in the cavity. In addition, as the inclination angle α increases, the temperature of the fluid decreases.

Fig. 4 displays steady-state contours for the streamlines and isotherms for various values of α ($0.0, \pi/4, \pi/2$) with $Ra = 1000$ and $Ha = 0.5$. By comparison of Fig. 4 with Fig. 3, one can understand the effect of increasing the Rayleigh number on the streamline and isotherm contours. This comparison shows that as the Rayleigh number increases, stronger convective clockwise and anti-clockwise motion takes place in the cavity and the temperature gradient gets crowded at the walls of the cavity more than the previous case ($Ra = 500$). This, in general, causes reduction in the fluid temperature profiles.

Figs. 5 and 6 show comparison between the steady-state contours for the streamlines and isotherms for $\alpha = \pi/4$ with $Ra = 5 \times 10^3$ in the presence and absence of the magnetic field force. From this comparison, we can conclude that the intensity of the convection in the core of the cavity is considerably affected by the magnetic field. A weak convective motion is observed in the case of the presence of the magnetic field so we can say that, the absence of the magnetic force tends to accelerate the fluid motion inside the cavity. However, the absence of the magnetic field leads to decrease in the temperature of the fluid.

Fig. 7 illustrates the effects of the Hartmann number Ha and Rayleigh number Ra on the profiles of the X -component of velocity at mid-section of the cavity for different values of inclination angle α . The results show that increasing the values of the Rayleigh

Fig. 3. Streamlines and isotherms for $Ra = 500$ and $Ha = 0.5$.

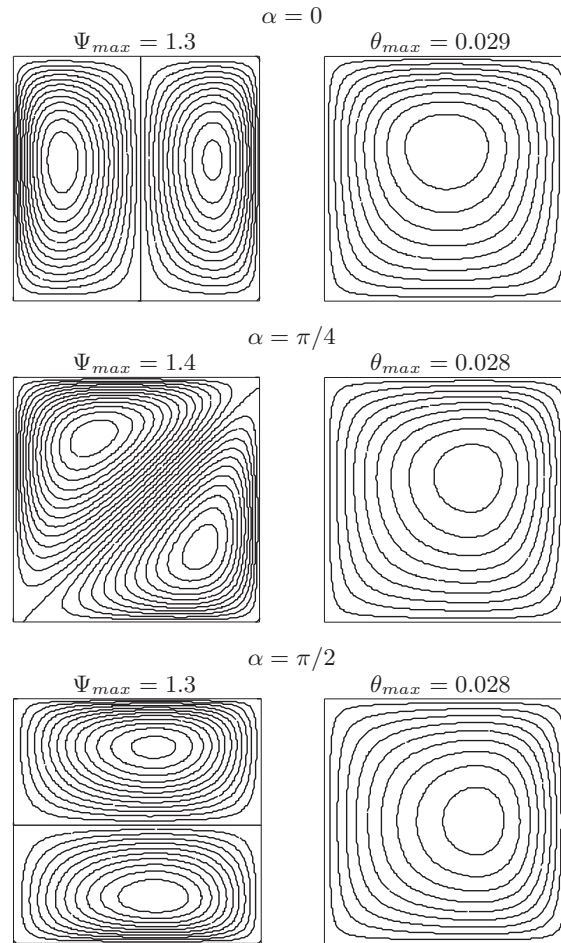


Fig. 4. Streamlines and isotherms for $Ra = 1000$ and $Ha = 0.5$.

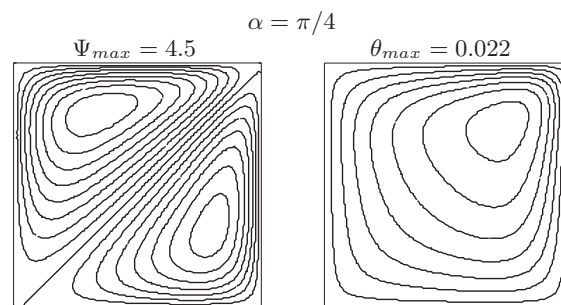


Fig. 5. Streamlines and isotherms for $Ra = 5000$ and $Ha = 0.5$.

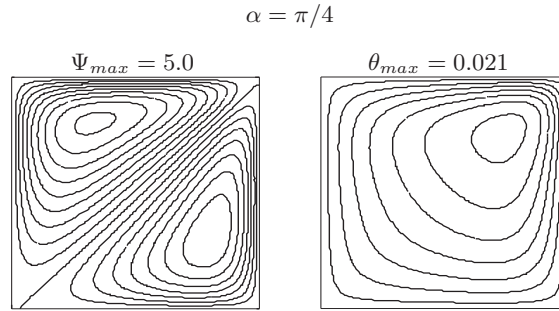


Fig. 6. Streamlines and isotherms for $Ra = 5000$ and $Ha = 0$.

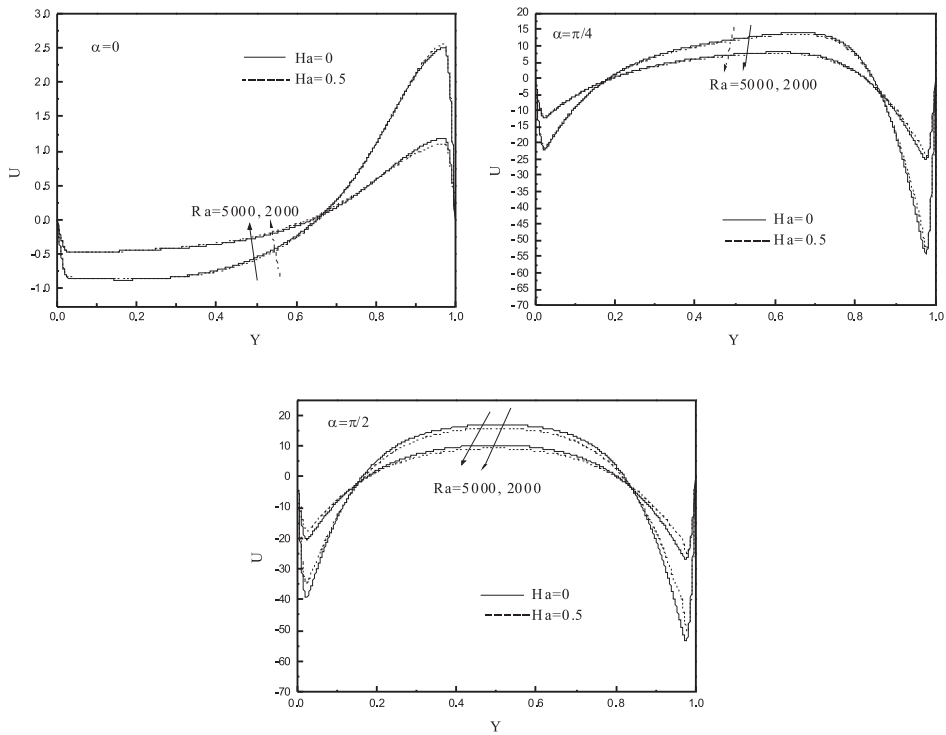


Fig. 7. Effects of Hartmann number Ha and Rayleigh number Ra on X -component of velocity at cavity mid-section for different values of angle α .

number Ra results in an increase in the fluid X -component of velocity whereas the X -component of velocity can be reduced by increasing of the Hartmann number Ha . The same behavior is observed when we studied these effects on the profiles of the fluid Y -component of velocity, see Fig. 8.

The temperature profiles at mid-section of the cavity for different values of angle α are depicted in Fig. 9. In this figure, the temperature of the fluid decrease by increasing the Rayleigh number as well as it takes the same behavior when the magnetic field increases.

The effects of the inclination of the cavity, presence of magnetic field force and the Rayleigh number on the average Nusselt number for unsteady and steady states are displayed in Tables 1–3. It is clear from these tables that when the inclination angle of the cavity and Hartmann number increase, the values of the average Nusselt number increase. Also, the same behavior is observed when the dimensionless time parameter increases. However, the opposite effect or behavior is predicted whereby the average Nusselt number decreases when the Rayleigh number increases. These behaviors are clearly depicted in Tables 1–3.

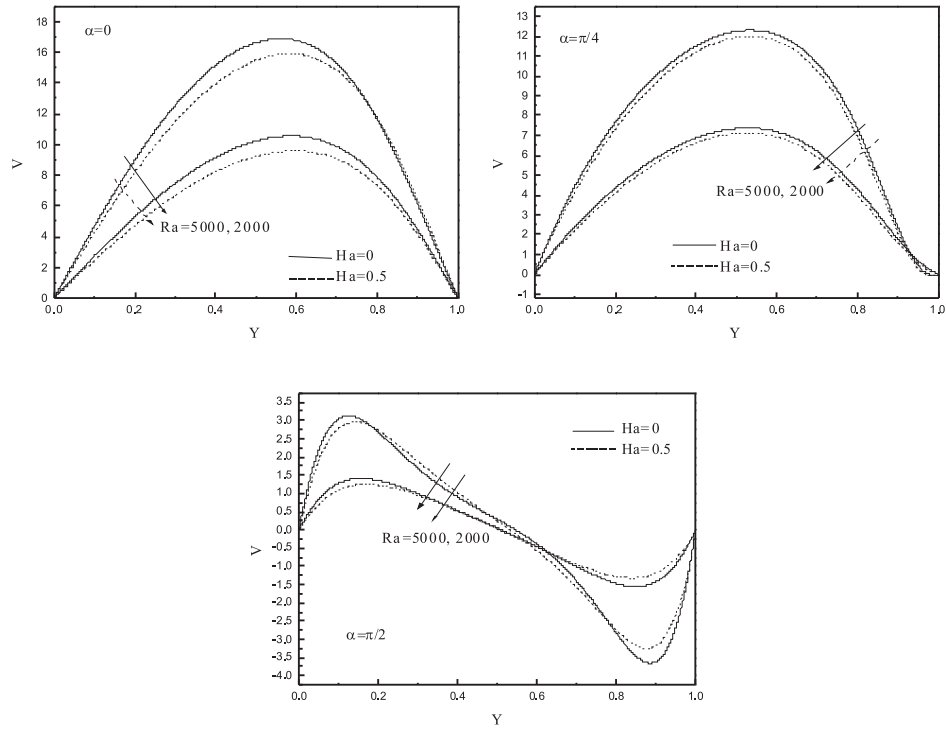


Fig. 8. Effects of Hartmann number Ha and Rayleigh number Ra on Y -component of velocity at cavity mid-section for different values of angle α .

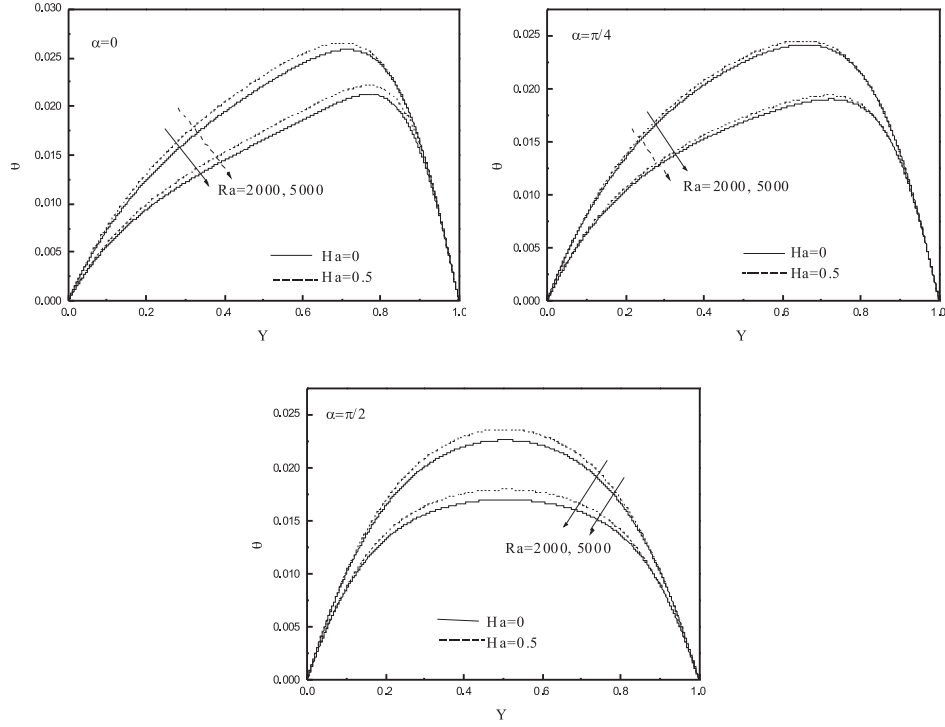


Fig. 9. Effects of Hartmann number Ha and Rayleigh number Ra on temperature profiles at cavity mid-section for different values of angle α .

Table 1. Values of average Nusselt number at the right wall for different values of α and τ when $Ra = 5 \times 10^3$, $Ha = 0.5$.

α	τ	\overline{Nu}
0	0.001	0.0147391
	0.005	0.0292422
	0.1	0.0622076
	Steady state	0.0622483
$\pi/4$	0.001	0.0147396
	0.05	0.0652462
	0.1	0.0670606
	Steady state	0.0671578
$\pi/2$	0.001	0.0147415
	0.05	0.0785632
	0.1	0.0905655
	Steady state	0.0916340

Table 2. Values of average Nusselt number at the right wall for different values of Ha and τ when $Ra = 5 \times 10^3$, $\alpha = \pi/4$.

Ha	τ	\overline{Nu}
0	0.001	0.0147409
	0.05	0.0713141
	0.1	0.0769137
	Steady state	0.0776113
0.5	0.001	0.0147409
	0.05	0.0718361
	0.1	0.0780096
	Steady state	0.0788913
1.0	0.001	0.0147410
	0.05	0.0730152
	0.1	0.0805914
	Steady state	0.0820411

Table 3. Values of average Nusselt number at the right wall for different values of Ra and τ when $Ha = 0.5$, $\alpha = \pi/4$.

Ra	τ	\overline{Nu}
1000	0.001	0.0147414
	0.05	0.0746656
	0.1	0.0846579
	Steady state	0.0847942
2000	0.001	0.0147409
	0.05	0.0718361
	0.1	0.0780096
	Steady state	0.0788913
5000	0.001	0.0147396
	0.05	0.0652462
	0.1	0.0670606
	Steady state	0.0671578

Case 2: The cavity vertical walls are adiabatic

To complete our discussion, we investigated the case when the enclosure vertical walls are adiabatic. From Fig. 10, we can observe the shapes of streamlines and isotherms contours for different values of the dimensionless time parameter τ when $Ra = 1000$, $\alpha = \pi/4$ and $Ha = 0.5$. It is clear that the fluid moves from the core of the enclosure to the vertical walls forming two symmetrical clockwise and anti-clockwise circular cells with maximum value $\Psi_{max} = 0.65$ at $\tau = 0.05$. As the dimensionless time parameter increases, the clockwise contours increase and the maximum value of stream function

increases until it reaches the fixed value $\Psi_{max} = 2.0$ at the steady-state condition. Also, the constant temperature lines or isotherms turn from parallel lines with maximum value $\theta_{max} = 0.017$ at $\tau = 0.05$ to curves with maximum value $\theta_{max} = 0.042$ at steady state.

Figs. 11–13 display the effect of the dimensionless time parameter τ on the velocity components in the X - and Y -directions and the temperature profiles at the enclosure mid-section when $Ra = 5 \times 10^3$, $\alpha = \pi/4$ and $Ha = 0.5$. It is found that, as the dimensionless time parameter τ increases, the velocity components U and V increase until they reach fixed values at the steady state condition. Also, the same behaviors are observed for the temperature distributions. In addition, the values of the average Nusselt number for the unsteady and steady-state conditions are shown in Table 4. From this table, we can observe that as the dimensionless time parameter increases, the average Nusselt number decreases until it reaches the minimum value at steady state.

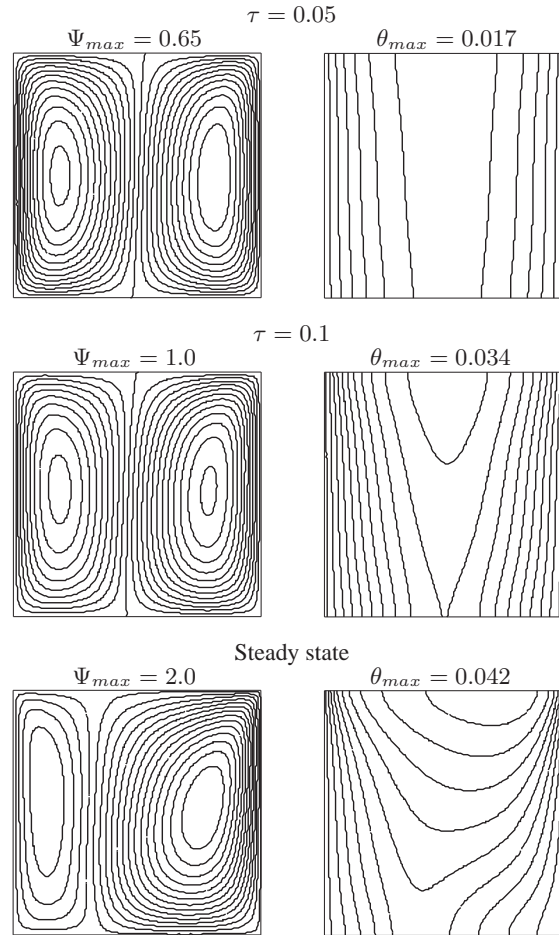


Fig. 10. Streamlines and isotherms for $Ra = 1000$, $\alpha = \pi/4$ and $Ha = 0.5$.

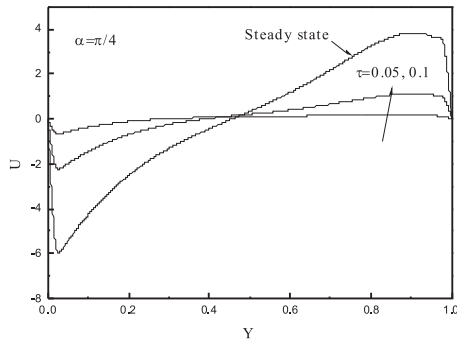


Fig. 11. Effects of the dimensionless time parameter τ on X -component of velocity at cavity mid-section.

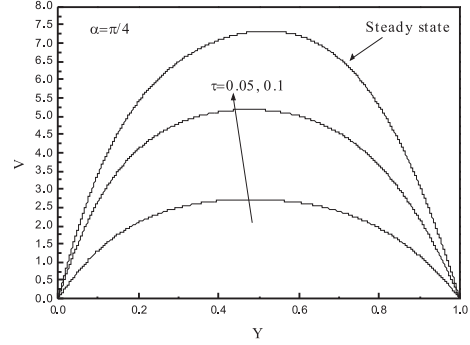


Fig. 12. Effects of the dimensionless time parameter τ on Y -component of velocity at cavity mid-section.

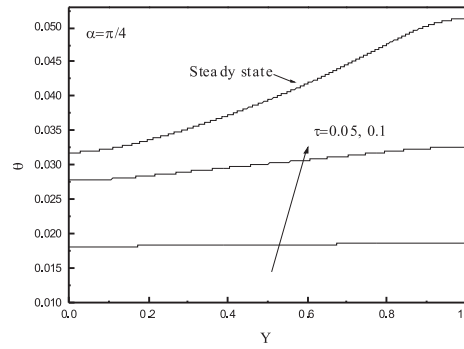


Fig. 13. Effects of the dimensionless time parameter τ on temperature profiles at cavity mid-section.

Table 4. Values of average Nusselt number at the right wall for different values of α and τ when $Ra = 5 \times 10^3$, $Ha = 0.5$.

α	τ	\overline{Nu}
$\pi/4$	0.001	0.0003385
	0.005	0.0003094
	0.05	0.0001513
	0.1	0.0000536
Steady state		0.0

5 Conclusions

In the present paper, we have studied the transient MHD natural convection in an inclined cavity filled with a fluid saturated porous medium by including the effects of presence both of an inclined magnetic field and heat source in the solid phase. We have examined the effects of Rayleigh number, Hartmann number as well as values of inclination angle of the cavity, various values of the dimensionless time parameter and magnetic field on the flow and heat transfer characteristics for the case of cavity with cooled walls and the case of cavity with adiabatic vertical walls. From this investigation, we can draw the following conclusion:

1. In general, we can increase the temperature of the fluid by increasing both of the magnetic field force and the inclination angle α .
2. The various values of the inclination angle α affect on the streamline contours. These contours rotate and crowded at different walls by increasing of α .
3. A faster motion is considered when Rayleigh number increases whereas it causing in the decreasing of the temperature.
4. The average Nusselt number must be affected by the presence of the magnetic field, it takes a large value in case of the presence of magnetic field.
5. When the vertical walls were considered adiabatic, the activity of the fluid and heat transfer characteristics increases by increasing the dimensionless time parameter.

References

1. A. Bejan, K.R. Khair, Heat and mass transfer by natural convection in a porous medium, *Int. Commun. Heat Mass*, **28**, pp. 909–918, 1985.
2. F.C. Lai, F.A. Kulacki, Non-Darcy mixed convection along a vertical wall in a saturated porous medium, *Int. J. Heat Mass Tran.*, **113**, pp. 252–255, 1991.
3. A.J. Chamkha, A. Khaled, Hydromantic coupled heat and mass transfer by natural convection from a permeable constant heat flux surface in porous media, *J. Porous Media*, **3**, pp. 259–266, 2000.
4. T.L. Bergman, F.P. Incropera, R. Viskanta, Correlation of mixed layers growth in double-diffusive, salt-stratified system heated from below, *J. Heat Transf.*, **108**, pp. 206–211, 1986.
5. J. Imberger, P.F. Hamblin, Dynamics of lakes, reservoirs, and coolingponds, *Annu. Rev. Fluid. Mech.*, **14**, pp. 153–187, 1982.
6. M.A. Stanish, G.S. Schager, F. Kayihan, A mathematical model of drying for hygroscopic porous media, *AIChE J.*, **32**, pp. 1301–1311, 1986.
7. P. Ratanadecho, K. Aoki, M. Akahori, A numerical and experimental study of microwave drying using a rectangular wave guide, *Dry. Technol.*, **19**(9), pp. 2209–2234, 2001.

8. P. Ratanadecho, K. Aoki, M. Akahori, Influence of irradiation time, particle sizes and initial moisture content during microwave drying of multi-layered capillary porous materials, *ASME J. Heat Trans.*, **124**(1), pp. 151–161, 2002.
9. P. Cheng, Heat transfer in geothermal systems, *Advances in Heat Transfer*, **4**, pp. 1–105, 1978.
10. P.H. Oosthuizen, H. Patrick, Natural convection in an inclined square enclosure partly filled with a porous medium and with a partially heated wall, *ASME Heat Transfer Division*, **302**, pp. 29–42, 1995.
11. P. Nithiarasu, K.N. Seetharamu, T. Sundararajan, Natural convective heat transfer in a fluid saturated variable porosity medium, *Int. J. Heat Mass Tran.*, **40**(16), pp. 3955–3967, 1997.
12. K.M. Khanafer, A.J. Chamkha, Mixed convection flow in a lid-driven enclosure filled with a fluid-saturated porous medium, *Int. J. Heat Mass Tran.*, **42**(13), pp. 2465–2481, 1998.
13. P. Nithiarasu, K.N. Seetharamu, T. Sundararajan, Numerical investigation of buoyancy driven flow in a fluid saturated non-Darcian porous medium, *Int. J. Heat Mass Tran.*, **42**(7), pp. 1205–1215, 1998.
14. T. Grosana, C. Revnicb, I. Popa, D.B. Ingham, Magnetic field and internal heat generation effects on the free convection in a rectangular cavity filled with a porous medium, *Int. J. Heat Mass Tran.*, **52**, pp. 1525–1533, 2009.
15. S. Akbala, F. Bayta, Effects of non-uniform porosity on double diffusive natural convection in a porous cavity with partially permeable wall, *Int. J. Therm. Sci.*, **47**, pp. 875–885, 2008.